Light Metals 2013 *Edited by: Barry Sadler*
TMS (The Minerals, Metals & Materials Society), 2013

GAS-SOLID FLOW APPLICATIONS FOR POWDER HANDLING IN ALUMINUM SMELTERS PROCESSES

Paulo Douglas S. de Vasconcelos[1], André L. Amarante Mesquita[2]
[1]Albras - Alumínio Brasileiro S/A, Barcarena-PA, Brazil
[2]Federal University of Pará, Belém-PA, Brazil.

Keywords: Gas-solid flow, Dense phase, Dilute phase, Minimum pressure drop, Minimum fluidization velocity

Abstract

Gas-solid flow occurs in many industrial furnace processes. The majority of chemical engineering unit operations, such as drying, separation, adsorption, pneumatic conveying, fluidization and filtration involve gas-solid flow.
Poor powder handling in an industrial furnace operation may result in a bad furnace performance, causing errors in the mass balance, erosion caused by particles impacts in the pipelines, attrition and elutriation of fines, overloading the bag houses. The lack of a good gas-solid flow rate measurement can cause economic and environmental problems due to airborne dust.
The paper is focused on the applications of powder handling in relation with furnaces of the aluminum smelter processes such as anode baking furnace and electrolytic furnace (pot cell) to produce primary aluminum.

Introduction

The anode baking furnace illustrated in figure 1 is composed by sections made up of six cells separated by partitions flue walls through which the furnace is fired to bake the anodes. The cell is about four meters deep and accommodates four layers of three anode blocks, around which petroleum coke is packed to avoid air oxidation and facilitate the heat transfer. During the baking process, the gases released are exhausted to the fume treatment center (FTC – [1]), where the gases are adsorbed in a dilute pneumatic conveyor and in an alumina fluidized bed. The handling of alumina is made via a dense phase conveyor.

Fig 1. Anode baking furnace building overview.

The baked anode is the positive pole of the electrolytic furnace (cell) which uses 18 of them by cell. The pot room and the overhead multipurpose crane are illustrated in figure 2.

The old aluminum smelters feed their electrolytic cells with the overhead cranes as can be seen in figures 2. This task is very hard to the operators and causes spillage of alumina to the pot room workplace. This nuisance problem is being solved by the development of a special multi-outlets nonmetallic fluidized pipeline [2].

Fig 2. Aluminum smelter pot room being fed of alumina by the multipurpose overhead crane.

The fundamentals of powder pneumatic conveying and fluidization will be discussed in this paper, such as the definition of a pneumatic conveying in dilute and dense phase, the fluidized bed regime map as illustrated in figure 3 and finally the air fluidized conveyor.

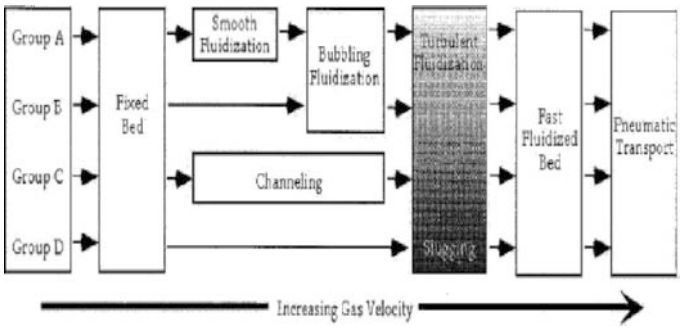

Fig 3. Flow regime map for various powders.

Firstly, petro coke and alumina used as raw materials in the primary aluminum process is characterized using sieve analyses (granulometry size distribution). Then, bulk and real density are determined in the laboratory analyses; with these powder physical

properties, they can be classified in four types using the Geldart's diagram as illustrated in figure 4 [3].
The majority of powders used in the aluminum smelters belong to groups A and B considering Geldart's criteria.
This figure 3 summarized the fluidized bed hydrodynamics related with powders classified according to Geldart's criteria.
Once the velocities associated with each mode of operation are determined, the pressure drop of the regime is calculated so that the gas-solid flow is predicted using the modeling and software adequate to optimize the industrial installation.
Finally one case study applied in the baking furnace of pneumatic powder conveying in dilute phase are shown as a result of a master degree dissertation. Another case study is the development of an equation to predict the mass solid flow rate of the air-fluidized conveyor as a result of a thesis of doctorate [2]. The equation has design proposal and it was used in the design of a fluidized bed to treat the gases from the bake furnace and for continuously alumina pot feeding the electrolyte furnaces to produce primary aluminum.

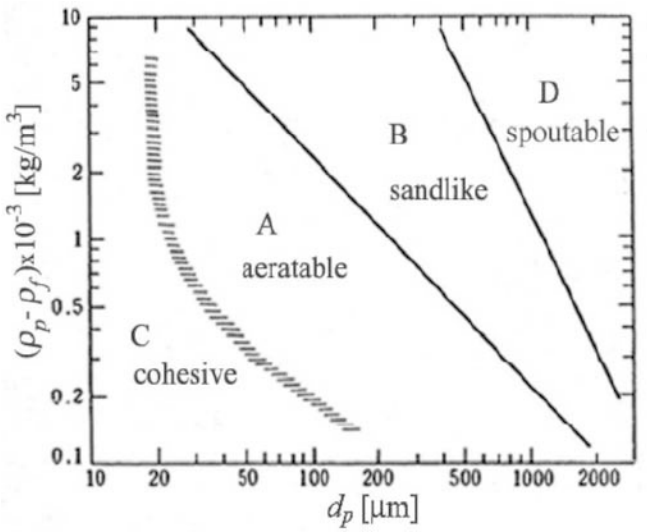

Fig 4. Powder classification diagram for fluidization by air – source: [3].

Fundamentals of pneumatic conveying of solids

Pneumatic conveying of solids is an engineering unit operation that involves the movement of millions of particles suspend by draft in dilute phase or in a block of bulk solids in dense phase inside a pipeline. Figure 5 illustrates a pneumatic conveying of solids with the essential components, like the air mover, feeding device, pipeline and bag house.
A good criterion showed in table 1 to decide if the transport of solids in air will be in dilute phase or in dense phase is the mass load ratio (μ) calculated by the equation 1.

$$\mu = \dot{G} / \dot{v}.\rho_g \qquad (1)$$

$\dot{G}$ Solid mass flow rate (kg/s)

$\dot{v}$ Gas (air) volume flow rate (m^3/s)

ρ_g Gas (air) density (kg/m^3)

Mode of transport of solids	Solids – to – air ratio (μ)
Dilute phase	0 - 15
Dense phase	> 15

Table 1 – Systems' classification concerning solids-to-air ratio - source: [4].

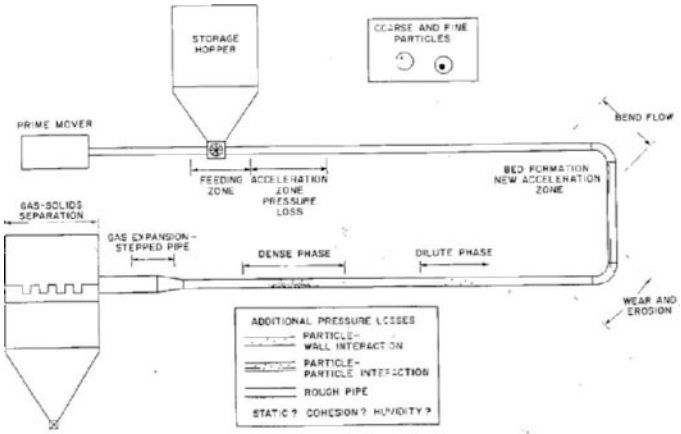

Fig. 5 – typical pneumatic conveyor layout – source: [4].

Figure 6 illustrates a variety of solids modes of transportation and the states diagrams showing the log of the pipeline pressure drop versus the log of the air velocity inside the pipeline. From figure 6 it is concluded that in dilute phase the pneumatic conveyor has high air velocity, low mass load ratio, and low pressure drop in the pipeline. In dense phase mode the conveyor operates with high mass load rate, low air velocity but high pressure drop in the pipeline. The engineer responsible for the project has to analyze which is the best solution for each case study.

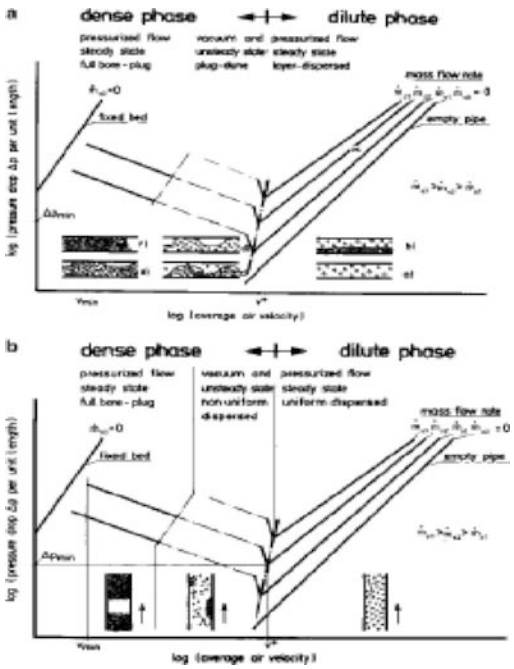

Fig. 6 – Conveying conditions showing the changes in solids loading; Vp: State diagram horizontal flow, down: State diagram vertical flow - source: [4].

Pressure drop calculation in the pipeline

The equations given here are based on the hypothesis that the gas-solid flow is in dilute phase. Some assumptions such as: transients in the flow (Basset forces) are not considered nor the pressure gradient around the particles (this is considered negligible in relation to the drag, gravitational and friction forces).
The pressure drop due to particle acceleration is not considered.
The flow is considering incompressible, Omni dimensional and the concentration of solids particles is uniform. The physical properties of the two phases are temperature dependent.
The mass flow rate for each phase can be expressed by the following equations:

$$\dot{m}_g = \rho_g . V_{mc} . \varepsilon_{mc} . A \quad (2)$$

$\dot{m}_g$ Gas mass flow rate (kg/s)
V_{mc} Minimum air velocity in dilute phase (m/s)
ε_{mc} Volume occupied by the gas inside the pipeline (-)
A_p Pipe cross section (m^2)

$$\dot{G} = \rho_s . V_s . \varepsilon_s . A_p \quad (3)$$

$$\varepsilon_s = \frac{A_s}{A_p} = \frac{4.\dot{G}}{\rho_s . \pi . D^2 . V_s} \quad (4)$$

$$\varepsilon_{mc} = \frac{A_g}{A_p} = 1 - \varepsilon_s \quad (5)$$

ρ_s Solid density (kg/m^3)
V_s Solid velocity (m/s)
ε_s Porosity or volume occupied by the solid inside the pipeline (-)
A_s Area occupied by the solid inside the pipeline (m^2)
A_g Area occupied by the gas inside the pipeline (m^2)
D Pipe diameter (m)

Velocity of the particle V_s and the particle terminal velocity V_t calculation:
In this paper it is considered the models of Yang [5] for the pressure drop calculation.

$$V_s = \frac{V_{mc}}{\varepsilon_{mc}} - V_t \sqrt{1 + \frac{2.f_s . V_s^2 . \varepsilon_{mc}^{4.7}}{g.D}} \quad (6)$$

$$V_t = \frac{g.d_p^2 . (\rho_s - \rho_g)}{18.\mu_g}, \quad K < 3.3 \quad (7)$$

$$V_t = \frac{0.153 . g^{0.71} . d_p^{1.14} . (\rho_s - \rho_g)^{0.71}}{\rho_g^{0.29} . \mu_g^{0.43}} \quad 3.3 < K < 43.6 \quad (8)$$

$$V_t = 1.74 . \sqrt{\frac{g.d_p . (\rho_s - \rho_g)}{\mu_g}}, \quad 43.6 < K < 2360 \quad (9)$$

K is a factor that determines the range of validation for the drag coefficient expressions, when the particle Reynolds number is unknown, and given by:

$$K = A_r^{1/3} = d_p . \left[\frac{g . \rho_g . (\rho_s - \rho_g)}{\mu_g^2} \right]^{1/3} \quad (10)$$

g Acceleration due to gravity (m/s^2)
d_p Particle diameter (m)
μ_g Gas dynamic viscosity ($Pa.s$)
f_s Solid friction factor (-)
A_r Archimedes' number (-)

The total pressure drop, ΔP_T for gas-solid flow is calculated with the contribution of the static pressure ΔP_E, and friction loss ΔP_F for both phases:

$$\Delta P_T = (\Delta P_E + \Delta P_F)_s + (\Delta P_E + \Delta P_F)_g \quad (11)$$

$$(\Delta P_E)_s = \rho_s . \varepsilon_s . L . g \quad (12)$$

$$(\Delta P_E)_g = \rho_g . \varepsilon_g . L . g \quad (13)$$

The contribution due to the friction factor given by the Darcy equation:

$$(\Delta P_F)_S = \frac{2.f_s . \rho_s . V_s^2 . L}{D} \quad (14)$$

$$(\Delta P_F)_g = \frac{2.f_g . \rho_g . V_g^2 . L}{D} \quad (15)$$

The friction factor for the gas is calculated by the Colebrook equation.

$$\frac{1}{\sqrt{4.f_g}} = 1.74 - 2.\log\left[2.\xi + \frac{18.7}{R_e . \sqrt{4.f_g}} \right] \quad (16)$$

$$R_e = \frac{\rho_g . V_{mc} . D}{\mu_g} \quad (17)$$

The friction factors due to solids in vertical and horizontal flow are obtained by the model of Yang [5].

$$f_{sv} = 0.00315 . \frac{1 - \varepsilon_{mc}}{\varepsilon_{mc}^3} \left[\frac{(1 - \varepsilon_{mc}) V_t}{V_{mc}/\varepsilon_{mc} - V_s} \right]^{-0.979} \quad (18)$$

$$f_{sh} = 0.0293.\frac{1-\varepsilon_{mc}}{\varepsilon_{mc}^3}.\left[\frac{(1-\varepsilon_{mc}).(V_g/\varepsilon_{mc})}{\sqrt{g.D}}\right]^{-1.15} \quad (19)$$

f_g Gas friction factor (-)

ξ Relative roughness of the pipe (-)

R_e Reynolds Number (-)

f_{sv} Friction factor due to solid in vertical flow (-)

f_{sh} Friction factor due to solid in horizontal flow (-)

Fundamentals of powder fluidization

Fluidization is an engineering unit operation that occurs when a fluid (liquid or gas) ascend trough a bed of particles, and that particles get a velocity of minimum fluidization V_{mf} enough to suspend the particles, but without carry them in the ascending flow. Since this moment the powder behaves like a liquid at boiling point, that is the reason for term "fluidization". Figure 7 gives a good understanding of the minimum fluidization velocity.

Minimum fluidization velocity calculation

In this paper it will be point out the beginning (fluidized bed) and the ending (pneumatic transport) of the flow regime map illustrated in figure 4.

The minimum fluidization velocity is calculated using the table 2 and its experimental value obtained using a permeameter.

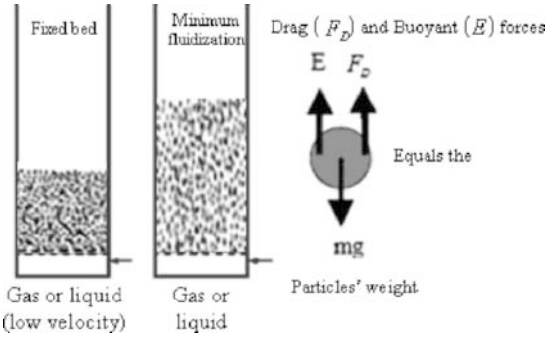

Figure 7 – Fixed and a fluidized bed of particles at a minimum fluidization velocity - adapted from Kunii and Levenspiel [6].

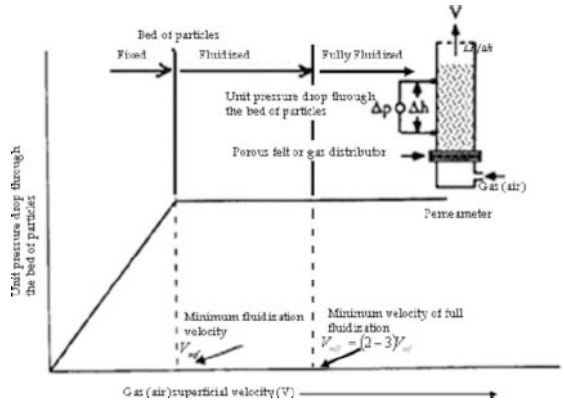

Figure 8 – Pressure drop through a bed of particles versus superficial air velocity – source: [7].

For an incipient fluidization, when the weight of particles equals the drag force, it is a good attempt to consider the porosity at the minimum fluidization velocity ε_{mf} equals the porosity ε of the fixed bed. The porosity of the fixed bed is calculated by the equation 27.

$$\varepsilon = 1 - \frac{\rho_{bnv}}{\rho_s} \quad (20)$$

$$\rho_{bnv} = \frac{M_s}{V_{total}} \quad (21)$$

$$\frac{1-\varepsilon}{\phi_s} = 0.255.Log(d_p) + 1.85 \quad (22)$$

ε Porosity or volume occupied by the solid in a bed of solids of a permeameter (-)

ε_{mf} Porosity of the fluidized bed of solids of the permeameter (-)

ρ_{bnv} Non-vibrated bulk density (kg/m^3)

M_s Mass of non-vibrated particles of volume V_{total} in a sample previously weighted (Kg)

V_{total} Total volume of particles and voids in the sample previously weighted (m^3)

ϕ_s Particle sphericity (-)

Table 2 – Semi-empirical equations to predict (V_{mf}) - source:[8].

Authors	Equation	
Abrahamsen & Geldart	$V_{mf} = 9x10^{-4} d_p^{1.8}\left[\lvert\rho_s - \rho_g\rvert g\right]^{0.934} \rho_g^{-0.066} \mu_g^{-0.87}$	(23)
Coltters and Rivas	$V_{mf} = 3.7774x10^{-5}\left(\frac{d_p^2 \lvert\rho_s - \rho_g\rvert g}{\mu_g}\left(\frac{\rho_s}{\rho_g}\right)^{1.23}\right)^{0.603559}$	(24)
Ergun simplified	$V_{mf} = \frac{(\rho_s - \rho_g).g.\varepsilon_{mf}^3.(\phi_s.d_p)^2}{150.(1-\varepsilon_{mf}).\mu_g}$	(25)
Leva	$V_{mf} = 9.23x10^{-3} d_p^{1.82}\left(\frac{\rho_g}{\mu_g}\right)^{0.88}\left(\frac{\rho_s}{\rho_g}\right)^{0.94}$	(26)
Miller and Logwinuk	$V_{mf} = 1.25x10^{-3}\left(\frac{d_p^2 \lvert\rho_s - \rho_g\rvert^{0.9} \rho_g^{1.1} g}{\mu_g}\right)$	(27)
Vasconcelos	$V_{mf} = 0.21 \lvert A_r\rvert^{0.25}\left(\frac{\phi_s}{1.05\varepsilon}\right)^{0.7} \lvert d_p g\rvert^{0.5}$	(28)
Wen and Yu	$V_{mf} = \frac{\mu_g}{\rho_g d_p} \lvert\sqrt{33.7^2 + 0.0408 A_r} - 33.7\rvert$	(29)

Petro coke handling at Albras anode bake furnace

Albras increased its productive capacity of 350,000 t/y to 390,000 t/y in the year 2000. To reach this production it was necessary to increase the bake furnaces capacity and, in consequence to increase the furnaces suction system capacity, which at that time didn't comply with efficiency the current demand of the plant. The Carbon Plant Engineering Group accepts the challenge to upgrade the original system to increase the coke suction capacity of 15 t/h

to 80 t/h. So software in FORTRAN was developed using the equations 1 to 19 to calculate the pressure drop in the circuit and to specify a new exhauster, redesign the bag house, the telescope tube and a new nozzle. Following, the steps of the project, from the coke characterization to a new circuit topology.
The system capacity was increased from 15 t/h to 110 t/h of coke suction capacity. Figure 9 shows the nozzle details of the old and new systems.

Figure 9 – Albras bake furnace coke suction system before and after modifications – source: [9].

Air fluidized conveyor (non-metallic round air slide)

It was developed a non-conventional air slide called air fluidized conveyor to be of low weight, non-electrical conductor, heat resistant, easy to install, maintain and also operates at a very low cost compared with the conventional metallic air slides. Figure 10 shows in the left a conventional air slide with rectangular shape, with one inlet and one outlet and in the right the round air fluidized conveyor with possibility to have multiples outlets.

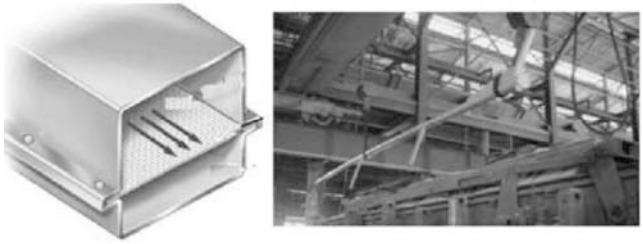

Figure 10 – The Albras aluminum smelter air fluidized conveyor and a conventional air slide in the left - source: [10].

Predict and experimental results of the air fluidized conveyor for reacted alumina

Two air-fluidized conveyors using the equation 30 were developed as result of a thesis for doctorate [2]. The results for the conveyor with diameter of 3 inches and 1.5 m long showed in figure 11 are summarized in table 4.

Figure 11 – Air-fluidized conveyor of 1.5 m long with three outlets - source [10].

$$\dot{G} = \left[\frac{(150.(1-\varepsilon_f)^3.\mu_g}{\varepsilon_f^3.(\phi_s.d_p)^2}.V.(sen\theta + \mu_a) + \frac{(1.75.(1-\varepsilon_f).\rho_g.}{\varepsilon_f^3.(\phi_s.d_p)}.V^2.(sen^2\theta + \mu_a.\cos\theta) + \rho_b.g.(2.sen\theta - \mu_a.\cos\theta) \right] . \left(\frac{v}{g} \right) \quad (30)$$

$$\mu_a = \tan\left[(1 - 0.01\frac{V}{V_{mff}})^2.\phi_i \right] \quad (31)$$

θ Angle of inclination of the air slide (°)

μ_a Coefficient of friction between particles and the bottom of the air slide (-)

ϕ_i Particles internal friction angle (°);

V, V_{mff} Superficial velocity of fluidization and minimum velocity of full fluidization (m/s)

Table 4 – Predicted solid mass flow rate based on equation 30 - source [10].

Mass gas-solid flow rate for alumina fluoride (t/h) - Air Fluidized conveyor of (3"/1.5m)							Inclinação (°)
0	0	0	2.1488	4.7091	6.173	7.978	(-1)
0	0	0	2.825	5.871	7.635	8.649	(-0.5)
0	0	0.944	3.563	6.448	8.099	8.851	0
0	1.293	3.529	4.952	7.787	8.917	9.127	1
0	2.778	4.261	6.002	8.478	10.523	10.309	2
0	3.1926	4.829	6.208	9.764	11.497	13.195	3
40	60	70	80	120	160	200	Air flow rate (LPM)
0.5	0.75	0.875	1	1.5	2	2.5	← V/V_{mff}

The experimental results for the air-fluidized conveyor showed in figure 14 are summarized in table 5.

Table 5 – Experimental results from the tests runs at Albras' laboratory - source [10].

Mass gas-solid flow rate for alumina fluoride (t/h) - Air Fluidized conveyor of (3"/1.5m)							Inclinação (°)
0	0	0.026	1.252	3.386	5.740	7.813	(-1)
0	0	0.132	1.380	3.562	5.962	8.075	(-0.5)
0	0	0.239	1.507	6.641	6.184	8.336	0
0	0	0.452	1.762	4.091	6.626	8.857	1
0	0	0.665	2.017	4.442	7.067	9.376	2
0	0	0.878	2.270	4.791	7.505	9.891	3
40	60	70	80	120	160	200	Air flow rate (LPM)
0.5	0.75	0.875	1	1.5	2	2.5	← V/V_{mff}

Figure 12 shows the other air-fluidized conveyor of 3 inches diameter and 9.3 m long designed using equation 30, which will be used as prototype to feed continuously the electrolyte furnace with reacted alumina.

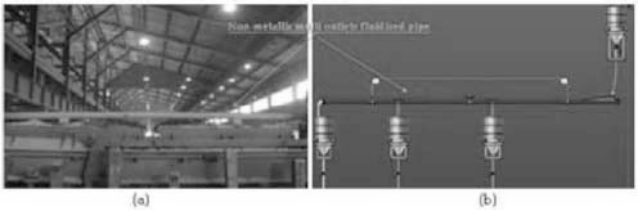

(a) (b)

Figure 12 – a) The nonmetallic fluidized pipe during tests at Albras; b) Sketch of the nonmetallic fluidized pipe for performance test at the fluidization laboratory - source [10].

The equation 30 predicts a mass solid flow rate of 7.29 t/h for that conveyor, but observed was a mass solid flow rate of 6.6 t/h at $1.5\,V_{mff}$ and a downward inclination of 0.5° was used during the test run depicted in figure 13.

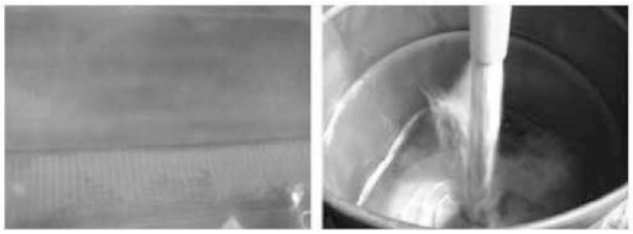

Figure 13 – Test rig of a 3"/9.3 m long round air slide at Albras - source [10].

Conclusions

The objective of this paper is to contribute with readers responsible for the design and operation of industrial furnaces. Focused on the project of powder handling at high velocity, such as the case study concerning pneumatic conveying in dilute phase applied at Albras aluminum smelter. The last case study regarding powder handling at very low velocity such is illustrated in figure 3 is used in several industrial applications and the intention in this case is to help project engineers to design air slides of low energy consumption. Based on the desired solid mass flow rate of the process using equation 30 is possible to design the conveyor, knowing the rheology of the powder that will be conveyed. In the application of Albras aluminum smelter the experiments results for the small conveyor the values obtained in the experiments was higher than that predict for horizontal and upward inclination in velocities less than the minimum fluidization velocity, because the equation doesn't take in to account the height of material in the feeding bin. In the case of the larger conveyor we have better results, because the conveyor is fed by a fluidized hose as can be seen in figure 12b. So in the next steps of the research it will be necessary to include the column of the feeding pipe/bin in equation 30.

References

1. Vasconcelos, P.D., and Mesquita, A.L., Development of a New Improved Dry Alumina Scrubber for Emission Control from Anode Bake Furnaces - Light Metals 2010, pp. 583-588.
2. Vasconcelos, P.D., Doctorate Thesis, Federal University of Pará at Belém, 2011
3. Geldart, D., Types of Gas Fluidization Powder Technology, 7, 285 – 292 (1972).
4. Klinzing, G. E., Marcus, R. D., Risk, F., and Leung, L. S., Pneumatic Conveying of Solids – A Theoretical and Practical Approach, second edition, Chapman Hall. (1997).
5. Yang, W. C., A mathematical definition of choking phenomenon and a mathematical model for predicting choking velocity and choking voidage, AIChE J., Vol. 21, 1013 (1978).
6. Kunii, D., and Levenspiel O., Fluidization Engineering, second edition, Butterworth-Heinemann, Boston (1991). Misra, C, Private Communication, Dec 2004.
7. Mills, D. Pneumatic Conveying Design Guide, Butterworths, London, (1990).
8. Vasconcelos, P.D., and Mesquita, A.L., Experimental and Theoretical Study on the Fluidization of Alumina Fluoride Used in the Aluminum Smelter Processes - Light Metals 2012, pp. 821-826
9. Vasconcelos, P.D., Improvements in the Albras Bake Furnaces Packing and Unpacking System – Light Metals 2000, pp. 493 – 497.
10. Vasconcelos, P.D., and Mesquita, A.L., Gas-solid flow applications for powder handling in industrial furnaces operations. Chapter 10, ISBN 978-953-307-585-3. Intech open access Publisher, Rijeka, September (2011).